Change Detection from SFM – The Impact of Repeat Station Imaging

Report for the Marshall Plan Foundation

Andrew C. Loerch, Dr. Gernot Paulus, Dr. Christopher D. Lippitt

10/16/2016

Table of Contents

Abstract

An adaptation of Repeat Station Imaging is compared with non-repeated flight line imaging to assess the methods' effects on vertical change detection accuracy. Structure from motion is used to create three-dimensional surface reconstructions of the study area, at four different point-cloud density levels, using imagery captured by an unmanned aerial vehicle. Boxes were deployed throughout the study area, and manipulated to create changes between the first and second flight. Four flights were performed, a baseline flight, an adapted Repeat Station Imaging flight, and two non-repeated flight line flights. Results indicate that the Repeat Station Imaging method produces more consistent systematic vertical change errors in

unchanged features but does not necessarily produce higher-accuracy change detection results consistently across all objects.

Acknowledgements

I would like to thank and acknowledge, foremost, the Marshall Plan Foundation for funding this research. The Marshall Plan Foundation offers fellowships to graduate students throughout Austria and the United States of America, to facilitate knowledge generation and cultural exchange.

Dr. Gernot Paulus, my sponsor and supervisor, is an outstanding researcher in geographic information science. In addition to providing the platform and facilities for this research, Dr. Paulus was instrumental in helping with the adjustments of living abroad.

Dr. Christopher Lippitt has been a motivational advisor throughout my master's degree, and involved me in many projects external to my thesis. These projects have typically involved field work with unmanned aerial vehicles, real-time-kinematic global positioning receivers, balloons, and camera systems.

1. Introduction

Aerial Triangulation and Structure-from-Motion (SFM) make it possible to create digital surface models of landscapes. Modern improvements in delivery platforms, digital cameras, and software applications have made it possible to create these models with high spatial resolutions and high temporal frequency (Westoby et al. 2012; Turner, Lucieer, and Watson 2012). Detecting changes in imaged and modeled landscapes is often a primary focus of remote sensing acquisitions, and the decision of which acquisition method to use can impact the overall accuracy of the detected changes (Coulter, Stow, and Baer 2003).

This research addresses the question, "How do repeated view geometries (RVG) impact the accuracy of vertical change detection?" To answer this question, four Unmanned Aerial

Vehicle (UAV) flights were conducted near Villach, Austria, with a platform containing a precision real-time-kinematic (RTK) receiver.

Test flights were conducted to determine the capacity of the aerial platform to repeat flight lines and imaging locations. These results indicated that the platform can reproduce the image frame-centers between the initial flight and flight two at 4.22 m horizontal root-mean-square-error (RMSE) and 0.77 m vertical RMSE.

Prior to the first study flight, thirteen accurately and precisely measured stacks of boxes of varying dimensions were placed throughout the scene. Seven of these stacks of boxes were unmoved across all flights, to provide a calibration metric containing changes detected to boxes that had not changed.

The initial flight plan was conducted over the deployed boxes. After this initial flight, scene changes were implemented by removing some boxes and placing new boxes throughout the scene. The second flight was then conducted utilizing the same flight plan and aircraft/sensor settings as the first flight, to maintain, as closely as possible, the view geometries between images of the first and second flights. The third flight was flown over the area with the simulated changes, with a flight path rotated by thirty-degrees from the first and second flights, to ensure different view geometries of the boxes from the initial two flights. A fourth flight was conducted over the deployed changes with a flight plan rotated at sixty-degrees from the initial two flights. The imagery from each of the flights was processed identically within the structure-from-motion (SFM) software Agisoft Photoscan, using a portion of the RTK ground control points for georeferencing. The digital surface models created from the Agisoft Photoscan SFM processing were then used to measure the vertical changes made to boxes at the scene.

This research shows that repeated view geometries can be used for obtaining higher-accuracy vertical change detection results. Calibration of vertical change detection using changes to invariant features can improve the accuracies. Selection of the desired density of point cloud data during image processing also plays a role in both the absolute accuracy of the results and in the utility of repeated view geometries.

2. Background

Change detection is a fundamental use of remote sensing. To conduct accurate automatic or semi-automatic change detection in software, several considerations exist. This review looks at how change detection has evolved to include digital surface models created with structure-from-motion, and how different image acquisition methods are being used for change detection.

2.1 Change detection and traditional imaging

The concept of automatic change detection based on differences between time series of images has existed for decades. Various algorithms for detecting changes in urban environments, glacial systems, and landforms have been developed and employed with varying degrees of success (Sarkar and Boyer 1996; Jensen and Im 2007; Jung 2004; Song et al. 2001). These algorithms typically employ methods of change detection from two time periods of imagery that are reliant on external Digital Elevation Models (DEM), or from two time periods of imagery that are used for creating the DEMs and performing the change detection (Jensen and Im 2007; Jung 2004). Creating DEMs from the imagery requires the use of stereo-pairs, or images with sufficient overlap and sidelap that aerial triangulation can be performed on matching stationary features in the images (Lee et al. 2008). The recommended overlap and sidelap between images was traditionally 80% and 60%, although changes to these percentages, 80% and 75%, are currently recommended with the use of low-altitude UAV's (Zhang, Xiong, and Hao 2011).

The steps necessary in acquiring and preprocessing the imagery in order to create the DEMs, orthomosaics, and subsequent change detections are largely reliant on sufficient image overlap, and exact co-registration between time series (Lippitt, Stow, and Coulter 2015; Lee et al. 2008; Coulter, Stow, and Baer 2003; Stow 1999). The traditionally employed imaging method for acquiring sufficiently overlapping imagery is the use of a platform such as a manned/unmanned aerial vehicle, and a sensor that is designed to capture images based upon either time intervals or distance traveled intervals (Lippitt, Stow, and Coulter 2015). This method of acquiring images usually ensures sufficient overlap to create the DEMs and

orthomosaics, however, further processing is necessary to co-register the time series (Coulter, Stow, and Baer 2003; Stow 1999). It is often the case that subsequent flights/acquisitions over an area do not follow the same flight lines/headings as previous acquisitions. When using higher-resolution digital surface models that include features with significant vertical relief such as buildings, trees, etc., there are issues with this method of image acquisition and co-registration related to parallax between different time series (Lippitt, Stow, and Coulter 2015; Stow 1999). The distortions in vertical features and co-registration errors between time series and varied view geometries reduces the accuracy of automatic change detections of features at pixel-level scales (Coulter, Stow, and Baer 2003; Lippitt, Stow, and Coulter 2015; Stow 1999).

2.2 Change detection and repeated view geometries

Repeat Station Imaging is an alternative method for acquiring imagery for use in change detection. With RSI, the flight and imaging path is designed using GNSS waypoints, and the imaging sensor is triggered based on these waypoints (Lippitt, Stow, and Coulter 2015; Coulter, Stow, and Baer 2003). Provided the same imaging sensor is used across acquisitions, the result is "multitemporal imagery with matched view geometry" (Lippitt, Stow, and Coulter 2015). This method of image acquisition has been shown to result in horizontal spatial co-registrations between multitemporal image sets of between one to two pixels (Lippitt, Stow, and Coulter 2015; Coulter, Stow, and Baer 2003). Rapid change detection in the context of the existing RSI research has focused on automatic detection of horizontal changes between image pairs and between two-dimensional orthomosaics.

Considering the complex change detection algorithms described by Jensen and Jung, which are heavily reliant on accurate DEMs or DSMs that are either external to, or created from, the multitemporal image sets, it is logical to conclude improvements to the accuracies of the DEMs/DSMs should result in improvements in the accuracies of change detection methods that rely on the surface models. An outstanding question of RSI, which this research addresses, is whether repeated view geometries result in consistent vertical relief errors in features between time series, and therefore produce more accurate vertical measurements of feature changes.

3. Methods

This research employed an adaptation of RSI with a UAV and RTK system, to collect four time-series of imagery: a baseline image set, a repeated view geometry image set, and two non-repeated view geometry image sets. Cardboard moving boxes were used as the change objects. Agisoft Photoscan was used for the SFM image processing.

3.1 Scene selection and change-object deployment

Feistritz an der Geil is a small town with a model aircraft park, and is within a short drive of the Carinthia University of Applied Science. The park has been used previously by the university for imaging of a nearby river, the Geil, which is undergoing management changes to reduce channelization. This ongoing research includes a series of 3 permanent ground control markers. **Error! Reference source not found.** shows the research area, the model air park, and surrounding area. The image used in creation of Figure 1 is an orthomosaic created from the initial flight of this research. At the time of the flights, the temperature was 28 degrees Celsius, the winds were calm-to-light on ground, and there were no clouds directly over the study area.

Boxes of varying sizes were chosen as the objects to be deployed and manipulated between flights. Individual boxes, once assembled, are simple to measure precisely. They are lightweight, and can be quickly stacked and moved. To prevent stacked boxes from moving due to slight breezes, they were taped together with duct tape. Two sets of boxes each were stacked to create objects with six differing heights; twelve objects total. One set of boxes remained stationary throughout each of the flights, and the other set of boxes were manipulated by removing boxes to shorten their heights, and placing the removed boxes throughout the scene to create new objects. After manipulation, there were a total of nineteen objects deployed throughout the scene.

Figure 1: Study area at Feistritz an der Geil.

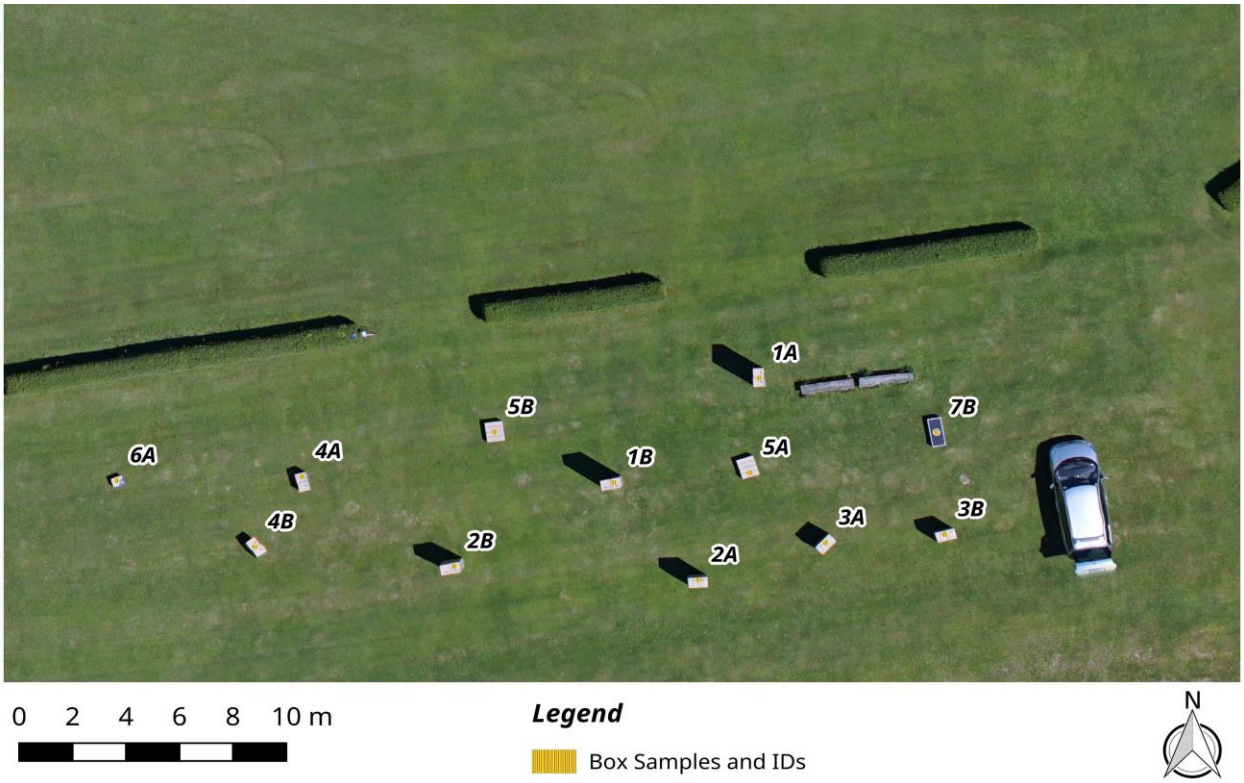

Figure 2: Object deployments, pre-change.

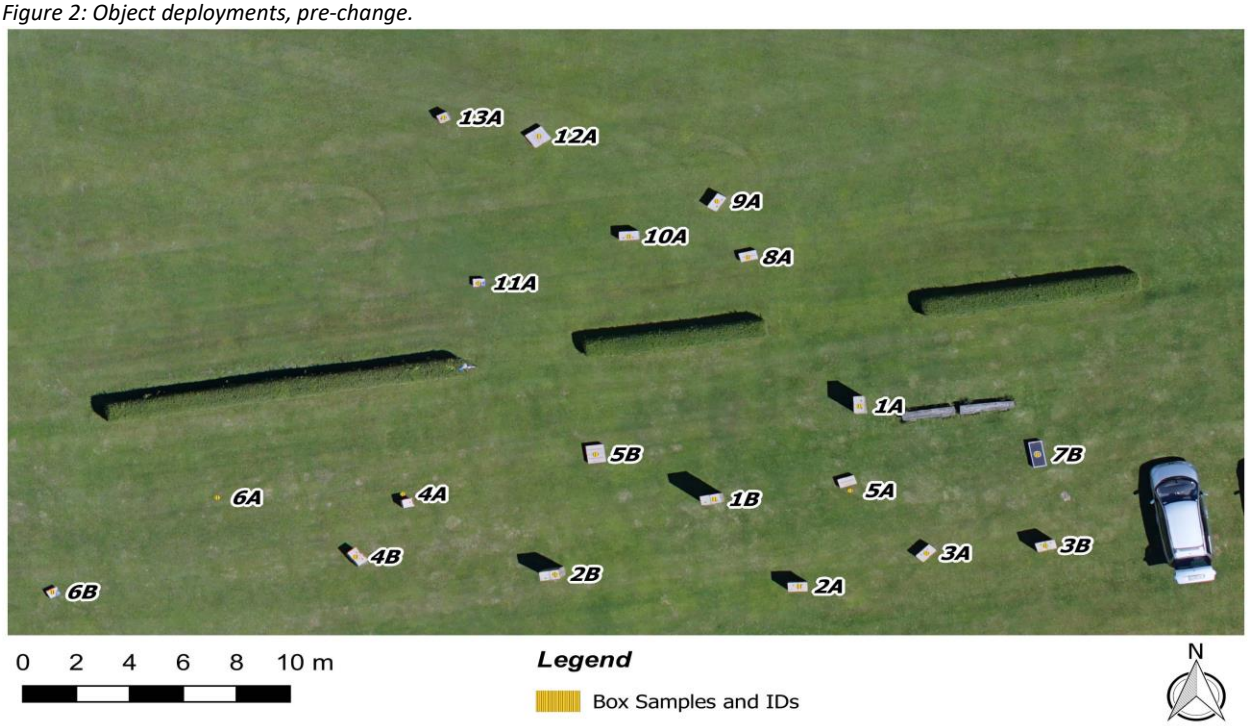

Figure 3: Object deployments, post-change.

Figure 2 illustrates the placement of boxes prior to manipulation. Figure 3 illustrates the placement of the objects after they were manipulated. Table 1 shows the initial object heights, and the vertical changes made to the objects, measured with a measuring tape.

Boxes ID	Initial Height (cm)	Change to height (cm)
1A	263.6	-65.9
1B	263.6	0.0
2A	197.7	-65.9
2B	197.7	0.0
3A	131.8	-65.9
3B	131.8	0.0
4A	65.9	-65.9
4B	65.9	0.0
5A	38.2	-38.2
5B	38.2	0.0
6A	28.2	-28.2
6B	28.2	0.0
7B	38.0	0.0
8A	0.0	38.2
9A	0.0	65.9
10A	0.0	65.9
11A	0.0	33.4
12A	0.0	38.2
13A	0.0	65.9

Table 1: Object IDs with associated starting heights and changes. Objects labeled with A are those that experienced a change after Flight 1. Objects 8-13 are the newly deployed boxes after Flight 1.

In both Figure 2 and Table 1, objects are given identification numbers. Objects labeled 1 through 7 were deployed prior to the initial flight. Objects 8 through 13 are those placed in the scene as new objects after the initial flight. Finally, the letter 'A' designates objects that were changed after the initial flight, and the letter 'B' designates those objects that remained unchanged across all flights. Object 7B is the only object used that was not a cardboard box; it is the UAV case.

3.2 Flight planning and image acquisition

The C-Astral Bramor rTK fixed-wing UAV was chosen as the acquisition platform. The Bramor has a 2.5 hour flight time, can carry larger mirrorless consumer cameras, and has a built in rTK receiver that communicates with a base station and is compatible with post-processing services (C-Astral 2015). The specified absolute dataset accuracy for this platform is 1.5cm. The available sensor system was a Sony a6000 mirrorless camera with a 30mm focal length lens. Figure 4 shows the platform ready for use at Feistritz an der Geil.

RSI based acquisitions are intended to match image-frame centers over time in order to reduce differences in view geometries (Coulter, Stow, and Baer 2003). It is preferable and simplest to accomplish RSI using waypoints as camera stations, and repeating those waypoints across acquisitions. The C-Astral Bramor, and many UAV and manned platforms, are designed

to use waypoints for navigation but not camera triggering (Coulter, Stow, and Baer 2003; Lippitt, Stow, and Coulter 2015; C-Astral 2015). Four flights were made to configure and test the Bramor system for waypoint-based camera triggering; these resulted in horizontal RMSE errors between repeated waypoints that were consistently greater than 5.5 m, with waypoints often missed entirely.

Figure 4: C-Astral Bramor RTK on-site at Feistritz an der Geil. Initial pre-change object deployment seen in background.

Because an objective of RSI is to obtain repeated view geometries and waypoint-based triggering was not an option, it was decided to create the initial flight plan using the Bramor's time-based camera triggering method. For the Bramor, this method works by initiating the camera triggering at the beginning of each flight line, and triggering every *x* number of seconds to achieve a specified overlap between images. To adapt the system and this research to the objectives of RSI, the second flight plan was kept identical to the first. This was intended to maintain the same heading, horizontal, and vertical locations where each image was captured between the initial and the second flight. Using this method, the horizontal RMSE of the

Figure 5: Initial object deployment, captured by initial flight.

Figure 6: Post-change object deployment, captured by flights 2-4.

repeated image locations is 4.22 m, and the vertical RMSE is 0.77 m. The defined horizontal velocity was 16 m/s and the defined altitude was 150 m. The values for desired overlap and sidelap were both set to 70%.

Figure 5 is a photograph of the distribution of the stacked boxes prior to the changes, which was flown for just the initial pre-change acquisition. You can see in this figure that there are no boxes across the hedge on the right-side of the photograph. Figure 6 is a photograph of the scene after the changes were implemented. Some stacks of boxes have been shortened in height, others removed, and new boxes are added that can be seen on the right side of the image.

Flight 3 was designed so that the flight path and therefore image orientations would be 30 degrees different from the initial flight. Additionally, no attempt was made to match the horizontal locations where the images were captured. Parameters for desired overlap and sidelap were kept the same as the initial flight. The closest horizontal distance between camera stations from the initial flight and Flight 3 over the deployed objects was 5.25 m, with an average heading difference of 30.64 degrees. The altitude was kept at 150 m, to avoid differences in scale.

Flight 4 was designed so that the flight path and therefore image orientations would be 60 degrees different from the initial flight. As with Flight 3, no attempt was made to match the horizontal locations where the images were captured, and parameters for desired overlap and sidelap were kept the same as the initial flight. The closest horizontal distance between camera stations from the initial flight and Flight 4 over the deployed objects was 7.36 m, with an average heading difference of 55.2 degrees. The altitude was kept at 150 m, to avoid differences in scale.

Figure 7 shows the three flights over the deployed objects, post-change, with the respective camera station locations. Although there is a noticeable difference between the initial flight paths and the ‘repeated’ flight path, that difference is clearly less than with the third and fourth flights, as noted above.

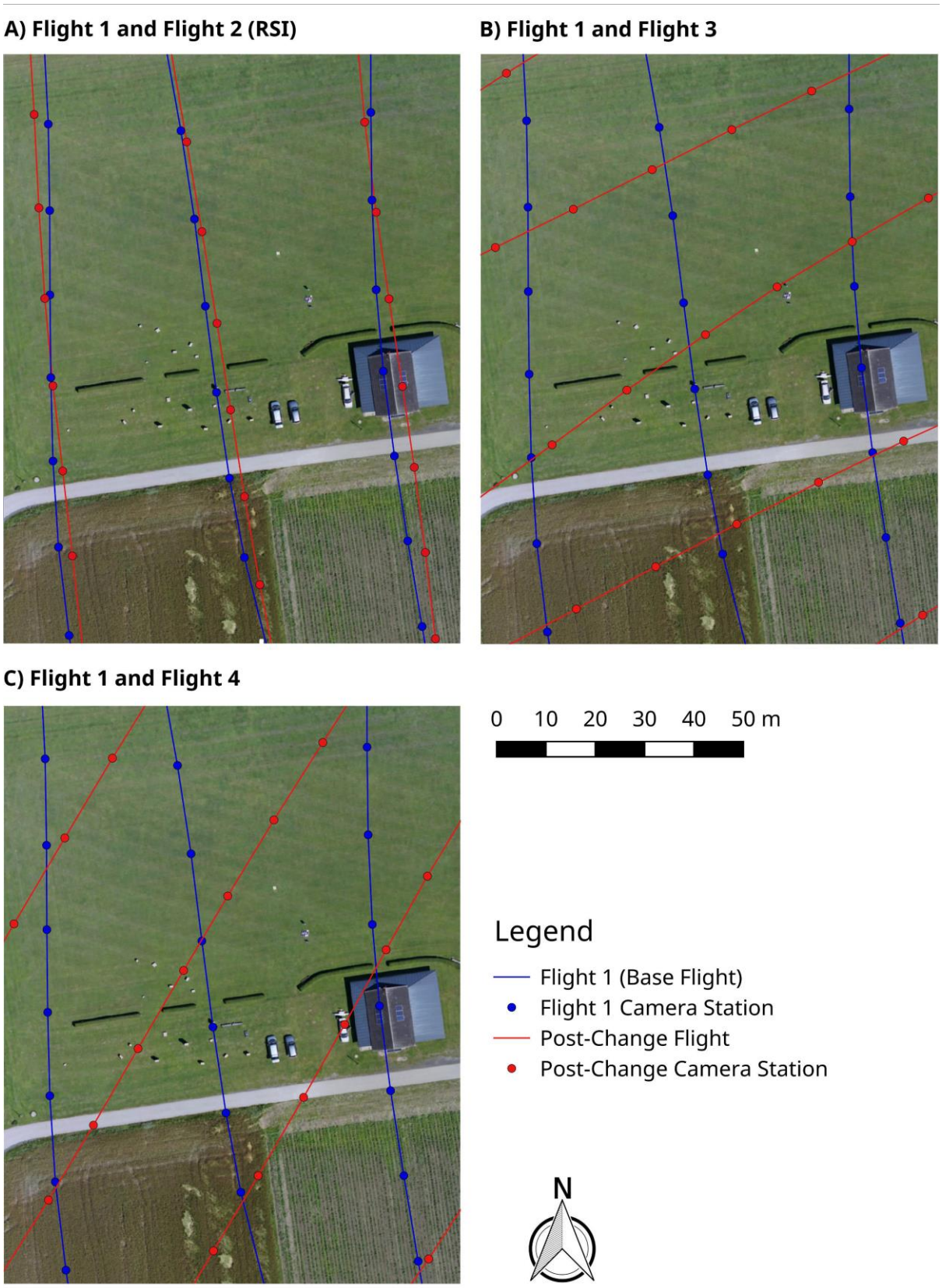

Figure 7: The four flight paths and camera locations, as flown. A) Shows the adapted RSI method, B) shows flight path shifted by 30 degrees compared to original, C) shows flight path shifted 60 degrees compared to original.

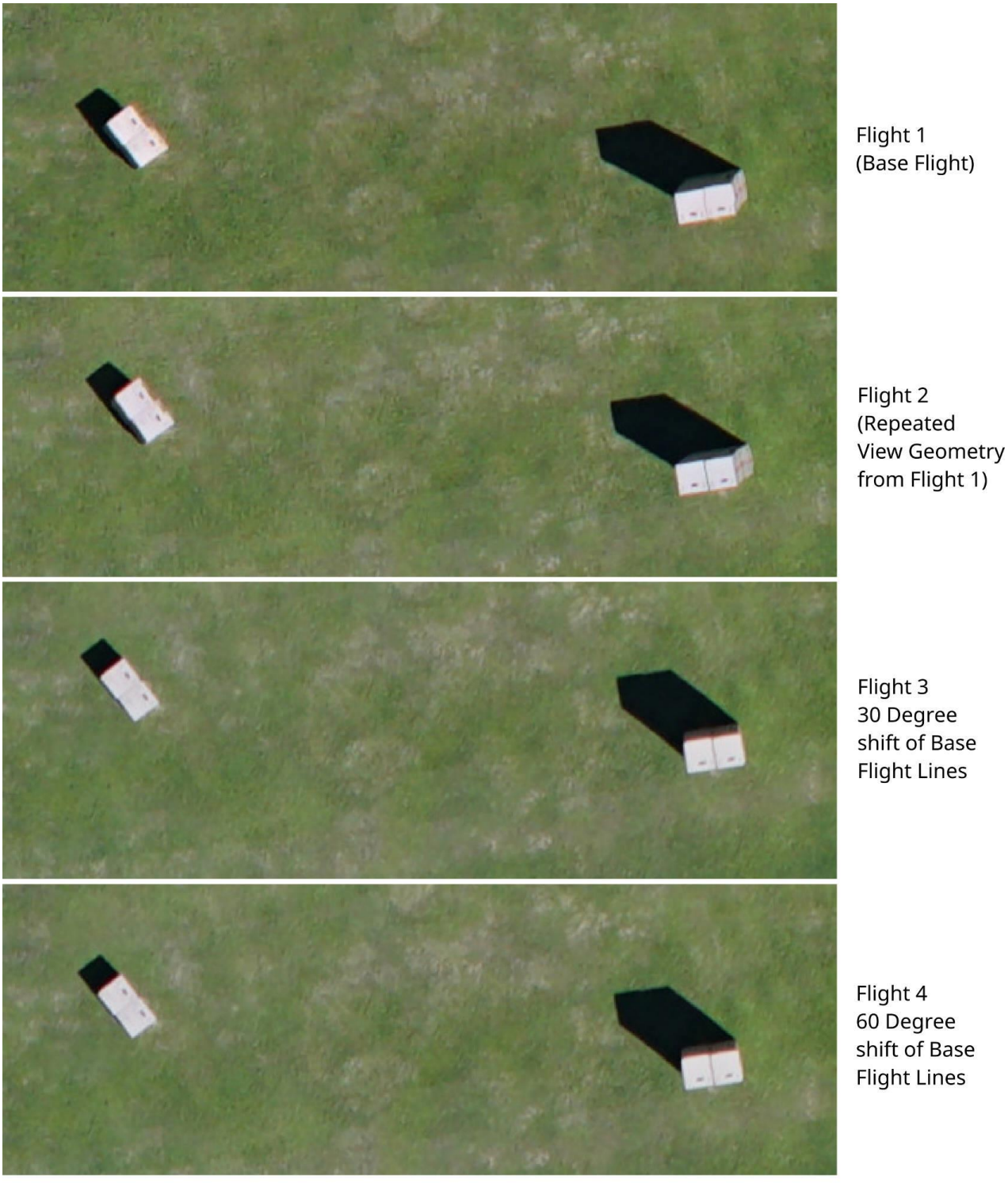

Figure 8: Examples of differences in object lean resulting from different view geometries, by flight.

With the given flight altitude of 150 m, and the Sony a6000 with the 30 mm lens, the imagery was collected at 1.95 cm Ground Sample Distance (GSD). In addition to the RTK-based image locations, six ground control points were collected with the C-Astral rTK rover, including the base station, with an absolute positional accuracy of 1.5 cm.

Figure 8 shows how the parallax, or lean, of the stacks of boxes appears to change between flights, dependent on view geometries. The object on the left side of this figure has a vertical height of 65.9 cm, and the object on the right has a vertical height of 197.7 cm. This figure clearly indicates that while Flight 2 does not perfectly repeat the view geometries of Flight 1, it is closer than Flight 3 and Flight 4 are to Flight 1.

3.3 Image Processing

Structure-from-motion image processing was conducted identically for each dataset using the Agisoft Photoscan workflow. Within Photoscan, four 'chunks', or groups of images, were created; one chunk per flight. Images for each flight were loaded into their respective chunks and the RTK image locations were loaded from the Bramor's logfile as reference data.

The six ground control points collected with the RTK rover were then loaded and identified in the imagery for each of the chunks/flights. Image alignment was performed on each flight. The low-accuracy tie points were discarded as follows: 1) points with a reconstruction uncertainty greater than or equal to 10%, 2) points with reprojection errors greater than 1%, 3) points with projection errors greater than or equal to 10%. After these tie-points were discarded, the image alignments were optimized.

Density Level	points/m²
Ultra-high	2600
High	643
Medium	162
Low	41

Table 2: The number of points per square meter associated with each density level.

After the alignment-step had completed for each of the four flights, the chunks were copied into four additional chunks. This was done so that each flight could be processed into an 'ultra-high', 'high', 'medium', and 'low' density point cloud, without introducing errors related to differences in alignments between the point cloud density levels. The point cloud densities for each of the four levels are shown in Table 2.

Figure 9:: Examples of the four different point cloud densities from Flight 2. A) Ultra-high density, B) High density, C) Medium density, D) Low density

Once the dense point clouds were created, the sixteen chunks (four flights and four point-cloud density levels) were then processed into DSMs and orthomosaics. T

Figure 9 shows an example of the four dense point clouds used for creating the digital surface models.

4. Analysis

The analysis of the impact of repeated view geometries on vertical change detection compared to traditional imaging involved comparisons between the DSMs, and accuracy assessments. This analysis assesses whether the closer view geometries between the initial flight and the second repeated view geometry acquisition produced more accurate vertical-change measurements than the comparison between the initial flight and subsequent non-repeated view geometry acquisitions. This analysis also looks at the effects of using the two acquisition methods with datasets derived from the four different point cloud densities.

4.1 Change Detection

Change detection can be performed using various methods, such as pixel differencing, direct object measurements, and hybrid approaches (Chen et al. 2012; Song et al. 2001; Stow 1999). Accurate DSM registration between the initial and subsequent flights is crucial for pixel differencing methods (Stow 1999). The imagery collected had a GSD of 1.96 cm, and the resultant GSD of the ultra-high density DSMs was 1.96 cm. Registration accuracies between the initial flight DSM and subsequent flight DSMs is shown for six points in Table 3.

	Flight 2 (cm)	Flight 3 (cm)	Flight 4 (cm)
point 1	1.0	2.0	1.6
point 2	2.4	1.1	2.7
point 3	2.1	0.8	3.9
point 4	3.6	3.6	3.8
point 5	0.1	2.9	2.6
point 6	1.4	1.6	1.6
RMSE	2.1	2.2	2.9

Table 3: DSM co-registration accuracies between initial and subsequent flights for six validation points.

The co-registration values between the flight DSMs is the result of the ground control points and RTK-based image location information used during the image processing step; no additional post-DSM-creation registration between flights was performed.

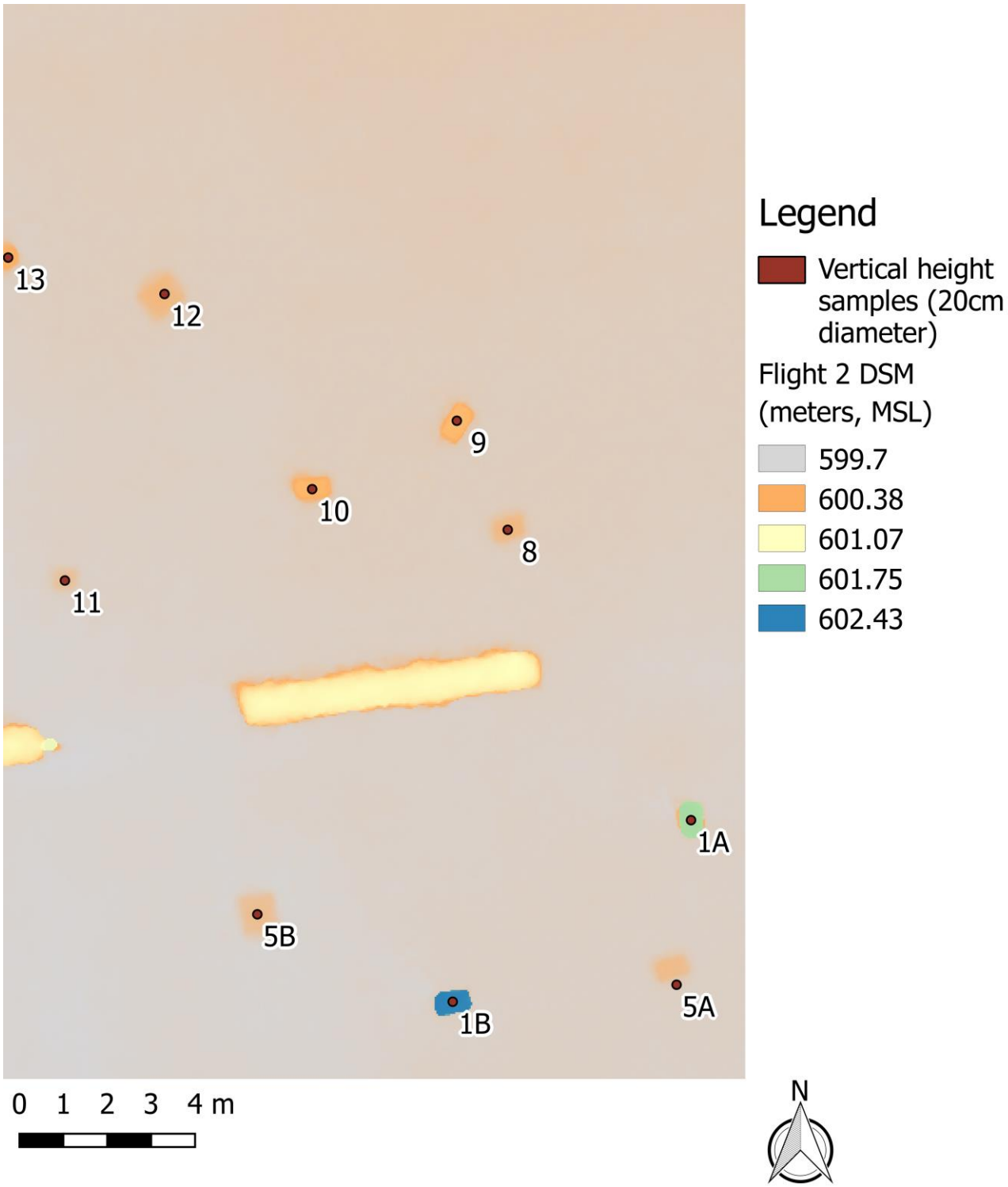

Figure 10: 20cm diameter samples used in calculating mean object heights are shown.

To assess just the vertical changes of the deployed objects, excluding areas where mis-registration results in horizontal, and therefore vertical, differences in the DSMs, each object

for each flight was individually characterized. The center pixel of each object was chosen, and 10 cm radius buffers were created around these pixels, resulting in 20 cm diameter samples of pixels. The mean pixel values were then calculated for each object, which represents the mean vertical heights of the objects. Figure 10 shows examples of the object samples used in calculating the object heights.

Change detection was then performed by subtracting the initial flight's median object heights from each of the post-change flights' median object heights. The resultant detected change values were then compared to the actual change values. This process was completed for each of the flights, for each of the designated density levels, resulting in twelve change detection values for each of the 19 objects.

4.2 Calibrating Change Detection Results

Of the 19 objects deployed for this study, 7 were kept stationary and 12 were manipulated by removing boxes from the stacks and adding them to the scene. The premise being tested by this design is that changes detected to unchanging objects are the result of error in the DSM, and that this error should be more consistent between flights with repeated view geometries and flights where the view geometries differed substantially.

The median change error detected for the unchanged objects for a given flight is subtracted from the change values for all objects for that flight, and the corrected change values are compared with both the actual changes and the uncorrected change values. The performance of this correction helps inform the answer to how RSI can impact vertical change detection from SFM products.

5. Results

The impacts of RSI on SFM for vertical change detection are presented in three contexts. The first context is the use of RSI where the change detection results are not calibrated by the changes detected to invariant objects. The second context is the use of RSI where changes are calibrated by using median changes detected to invariant objects. The third context is demonstrated alongside the first two, and it is the utility of RSI when different point cloud densities are used in creation of the digital surface models.

5.1 Uncalibrated Change Results

The adapted RSI acquisition accuracy outperformed the non-RSI acquisitions in the high and medium density vertical change detections by 0.4 cm and 0.7 cm respectively. It underperformed in the ultra-high and low density detections by 1.5 cm and 0.3 cm. The relationship between the detected vertical changes and the actual changes at each density are reported as adjusted r^2 values. The relationship between the RSI changes and the actual changes is slightly stronger at the high, medium, and low density products, and has no discernable difference compared to the other methods for the ultra-high density product. Table 4 shows the total RMSEs for each acquisition at each density, across all objects.

DSM Density & Flight #	Total RMSE (cm)	Total adj r^2
Ultra-High Density		
Flight 2	3.1	0.999
Flight 3	1.6	0.999
Flight 4	2	0.998
High Density		
Flight 2	3.7	0.997
Flight 3	4.1	0.993
Flight 4	4.2	0.992
Medium Density		
Flight 2	6.9	0.98
Flight 3	8	0.976
Flight 4	7.6	0.975
Low Density		
Flight 2	21.7	0.849
Flight 3	21.4	0.797
Flight 4	21.4	0.797

Table 4: Accuracy results and relationship strength between the actual changes made after the initial flight and the detected changes in the DSMs, shown by flights and density levels.

Tables 5-8 show the results of the vertical change detections for each of the 19 objects. The RMSEs for each acquisition at each density level correspond with those shown in Table 3.

Boxes ID	Initial Height (cm)	Actual Change (cm)	Flight 2 Error (cm)	Flight 3 Error (cm)	Flight 4 Error (cm)
1A	263.6	-65.9	3.1	0.3	0.0
1B	263.6	0.0	2.6	-1.3	1.0
2A	197.7	-65.9	2.4	1.1	1.0
2B	197.7	0.0	3.9	-0.3	1.7
3A	131.8	-65.9	3.7	-0.6	-0.2
3B	131.8	0.0	3.3	-1.4	0.0
4A	65.9	-65.9	2.7	2.5	0.1
4B	65.9	0.0	2.5	-1.2	0.7
5A	38.2	-38.2	6.6	1.7	6.9
5B	38.2	0.0	4.7	-1.5	-0.5
6A	28.2	-28.2	4.3	1.2	2.4
6B	28.2	0.0	0.0	-1.0	-0.9
7B	38.0	0.0	2.7	-0.8	0.4
8A	0.0	38.2	-0.4	-4.6	-2.4
9A	0.0	65.9	2.9	-1.2	0.1
10A	0.0	65.9	2.1	-0.6	-0.8
11A	0.0	33.4	0.4	-0.8	-1.8
12A	0.0	38.2	2.0	0.5	-1.1
13A	0.0	65.9	1.1	-1.5	-0.6
RMSE			**3.1**	**1.6**	**2.0**

Table 5: Individual object change accuracy results per flight. Ultra-high

Boxes ID	Initial Height (cm)	Actual Change (cm)	Flight 2 Error (cm)	Flight 3 Error (cm)	Flight 4 Error (cm)
1A	263.6	-65.9	2.9	-0.3	0.3
1B	263.6	0.0	2.6	-1.5	0.6
2A	197.7	-65.9	2.3	0.1	1.3
2B	197.7	0.0	5.6	0.5	2.5
3A	131.8	-65.9	2.5	-2.0	1.2
3B	131.8	0.0	3.3	-1.3	0.1
4A	65.9	-65.9	6.0	15.1	4.7
4B	65.9	0.0	3.0	1.6	0.2
5A	38.2	-38.2	10.8	6.2	15.2
5B	38.2	0.0	2.7	-0.9	0.0
6A	28.2	-28.2	0.7	0.0	-1.3
6B	28.2	0.0	1.2	0.9	0.2
7B	38.0	0.0	0.1	-2.3	-3.4
8A	0.0	38.2	-0.4	-2.9	-4.0
9A	0.0	65.9	2.4	-1.6	-0.9
10A	0.0	65.9	1.2	-2.7	0.4
11A	0.0	33.4	-2.9	-3.3	-4.6
12A	0.0	38.2	-1.9	-2.7	0.5
13A	0.0	65.9	-2.3	-2.3	-3.8
RMSE			**3.7**	**4.1**	**4.2**

Table 6: Individual object change accuracy results per flight. High density.

Figure 11 demonstrates the relationship between the actual, measured change values for the 19 objects and the change values derived from the DSMs. For each density listed besides the ultra-high density, the RSI-based flight had a closer relationship between the actual change values and the DSM-based change values.

At the ultra-high density level, the relationship difference between the acquisition methods is not discernable. The results of these relationship tests indicate that testing a calibration method is warranted.

5.2 Calibrated Change Results

Because the relationships between actual change values and the DSM-derived change values were stronger, especially at lower-densities, the change values for each object were adjusted by the median change value of the boxes that were kept stationary across all flights. This

Boxes ID	Initial Height (cm)	Actual Change (cm)	Flight 2 Error (cm)	Flight 3 Error (cm)	Flight 4 Error (cm)
1A	263.6	-65.9	2.0	-2.5	0.7
1B	263.6	0.0	3.8	-1.5	0.4
2A	197.7	-65.9	-0.9	0.5	1.5
2B	197.7	0.0	2.4	-5.0	-4.2
3A	131.8	-65.9	-2.9	-7.9	-10.0
3B	131.8	0.0	-5.8	-6.5	-2.2
4A	65.9	-65.9	18.5	17.3	14.9
4B	65.9	0.0	-2.8	-5.8	-5.7
5A	38.2	-38.2	16.9	13.7	17.4
5B	38.2	0.0	0.3	-1.3	0.0
6A	28.2	-28.2	-3.1	-2.5	-4.1
6B	28.2	0.0	0.6	1.1	-0.3
7B	38.0	0.0	-1.8	-8.8	-4.5
8A	0.0	38.2	-6.3	-7.4	-7.8
9A	0.0	65.9	-0.1	-8.0	-6.3
10A	0.0	65.9	-7.8	-11.7	-7.5
11A	0.0	33.4	-6.9	-7.2	-8.0
12A	0.0	38.2	-0.2	-2.1	-3.3
13A	0.0	65.9	-5.7	-12.5	-11.6
RMSE			**6.9**	**8.0**	**7.6**

Table 7: Individual object change accuracy results per flight. Medium density.

Boxes ID	Initial Height (cm)	Actual Change (cm)	Flight 2 Error (cm)	Flight 3 Error (cm)	Flight 4 Error (cm)
1A	263.6	-65.9	37.9	13.5	13.5
1B	263.6	0.0	4.5	-32.2	-32.2
2A	197.7	-65.9	-1.9	-26.5	-26.5
2B	197.7	0.0	9.7	1.1	1.1
3A	131.8	-65.9	11.7	9.0	9.0
3B	131.8	0.0	-2.5	-4.9	-4.9
4A	65.9	-65.9	56.0	51.6	51.6
4B	65.9	0.0	7.6	4.5	4.5
5A	38.2	-38.2	28.7	27.7	27.7
5B	38.2	0.0	6.3	2.4	2.4
6A	28.2	-28.2	4.8	0.7	0.7
6B	28.2	0.0	15.7	16.0	16.0
7B	38.0	0.0	6.9	-3.3	-3.3
8A	0.0	38.2	-16.5	-18.5	-18.5
9A	0.0	65.9	-14.1	-20.0	-20.0
10A	0.0	65.9	-23.5	-24.5	-24.5
11A	0.0	33.4	-14.3	-16.7	-16.7
12A	0.0	38.2	-14.2	-14.7	-14.7
13A	0.0	65.9	-37.6	-33.3	-33.3
RMSE			**21.7**	**21.4**	**21.4**

Table 8: Individual object change accuracy results per flight. Low density.

correction substantially improved the ultra-high density RMSE result for the RSI-based acquisition, from 3.1 cm to 1.6 cm.

For the high density, the correction improved the RMSE result for the RSI-based acquisition from 3.7 cm to 3.1 cm. At the medium density level, the correction to the RSI-based acquisition showed a decrease in change detection accuracy from 6.9 cm RMSE to 7.1 cm. At the lowest density level, the correction to the RSI-based acquisition improved the overall accuracy from 21.7 cm RMSE to 21.4 cm.

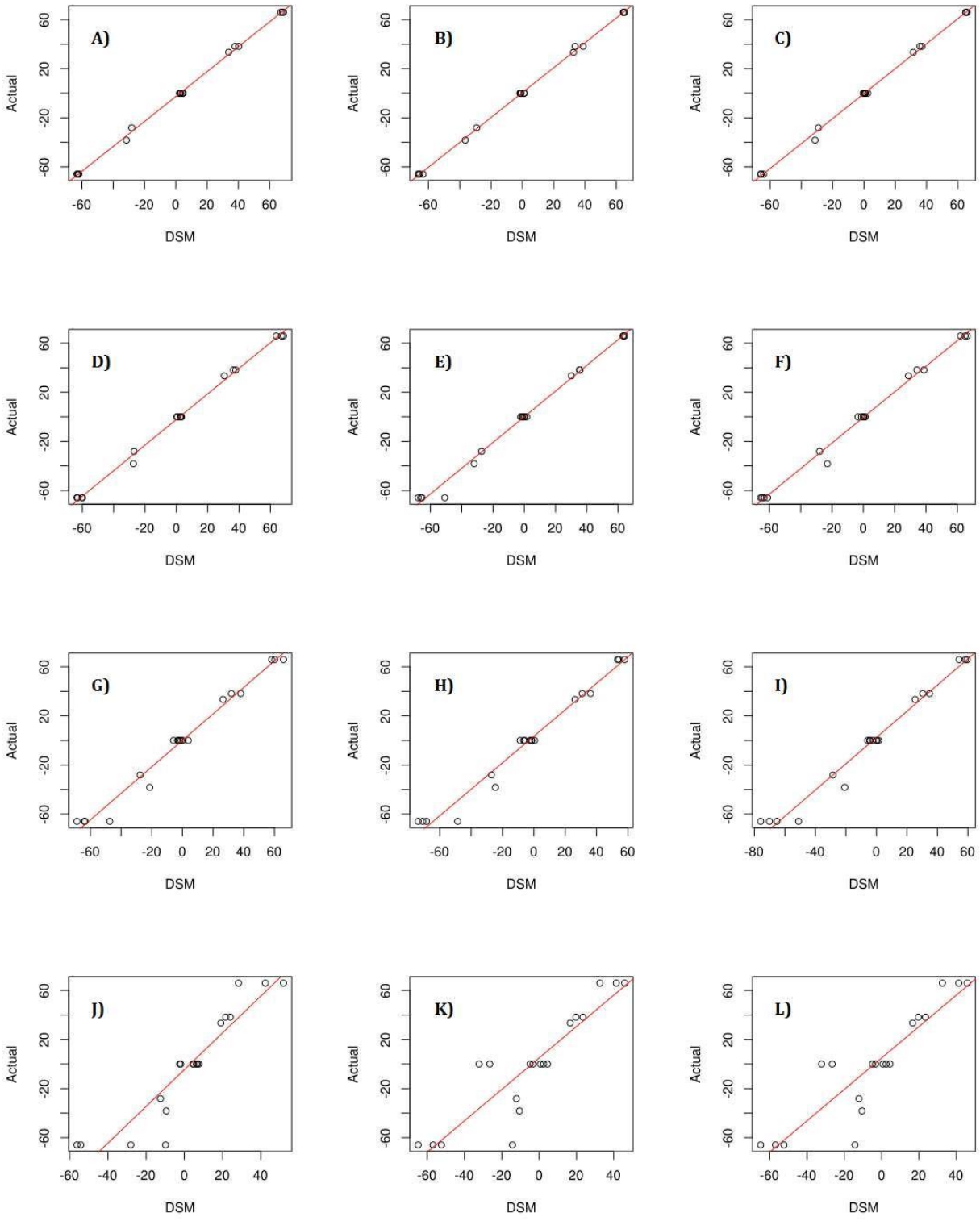

Figure 11: Relationships between actual change values of objects and DSM-derived change values. A-C are ultra-high density, flights 2-4, D-F are high-density, flights 2-4, G-I are medium-density, flights 2-4, J-L are low-density, flights 2-4.

For the ultra-high and high density levels with the non-RSI-based acquisitions, the overall RMSEs were unchanged with the corrections. At the medium density level, Flight 3 showed an RMSE improvement from 8.0 cm to 7.4 cm, and Flight 4 showed an RMSE improvement from 7.6 cm to 7.3 cm. At the lowest density level, Flight 3 and Flight 4 had improved RMSEs of 3 mm from the original results.

These results show that calibration of changes by using changes detected to unchanged features leads to generally better results for each of the image acquisition methods.

6. Conclusions

The accuracy of vertical change detections using very-high resolution ground sample distances with structure from motion processing was tested using two image acquisition methods. Repeat Station Imaging is a method that repeats image acquisitions using camera station GNSS coordinates, thereby repeating the view geometries of the scene as closely as possible. Our method adapted the goals of RSI to a fixed-wing UAV that does not trigger by GNSS coordinates, by repeating the flight headings, altitudes, and start and stop camera trigger points from the initial flight to the second flight. The second method of acquisition was intentional alteration of the flight headings and paths to create view geometries that were as different from the initial flight as possible, for the third and fourth flights.

Vertical change accuracies pre- and post-calibration are shown to be higher with the RVG acquisition method at the high and medium point cloud / DSM density levels. At the ultra-high point cloud / DSM density level, the RVG method performed as well as the altered-path methods, post-calibration.

This report does not specifically address the effects of an RVG-based method compared to non-RVG methods in terms of horizontal and volumetric accuracy. Initial observations from

the imagery collected for this research does indicate that further analysis of horizontal and volumetric accuracies are warranted.

7. References

C-Astral. 2015. “BRAMOR rTK.” Specification Sheet. Ajdovščina, Slovenia. http://www.c-astral.com/.

Chen, Gang, Geoffrey J Hay, Luis M T Carvalho, and Michael A Wulder. 2012. “Object-Based Change Detection” 33 (14): 4434–57.

Coulter, L.L., D.a. Stow, and S. Baer. 2003. “A Frame Center Matching Technique for Precise Registration of Multitemporal Airborne Frame Imagery.” *IEEE Transactions on Geoscience and Remote Sensing* 41 (11): 2436–44. doi:10.1109/TGRS.2003.819191.

Jensen, John R, and Jungho Im. 2007. “Remote Sensing Change Detection in Urban Environments.” Incollection. In *Geo-Spatial Technologies in Urban Environments*, 7–31. Springer.

Jung, Franck. 2004. “Detecting Building Changes from Multitemporal Aerial Stereopairs.” *ISPRS Journal of Photogrammetry and Remote Sensing* 58 (3–4): 187–201. doi:10.1016/j.isprsjprs.2003.09.005.

Lee, C Y, S D Jones, C J Bellman, and L Buxton. 2008. “Dem Creation of a Snow Covered Surface Using Digital Aerial Photography,” 831–36.

Lippitt, Christopher, Douglas Stow, and Lloyd Coulter. 2015. *Time-Sensitive Remote Sensing*. New York: Springer.

Sarkar, Sudeep, and K.L. Boyer. 1996. “Quantitative Measures of Change Based on Feature Organization: Eigenvalues and Eigenvectors.” *Proceedings CVPR IEEE Computer Society Conference on Computer Vision and Pattern Recognition*, 478–83. doi:10.1109/CVPR.1996.517115.

Song, Conghe, Curtis E. Woodcock, Karen C. Seto, Mary Pax Lenney, and Scott A. Macomber. 2001. “Classification and Change Detection Using Landsat TM Data: When and How to Correct Atmospheric Effects?” *Remote Sensing of Environment* 75 (2): 230–44. doi:10.1016/S0034-4257(00)00169-3.

Stow, D.A. 1999. “Reducing the Effect of Misregistration on Pixel Level Change Detection.” *International Journal of Remote Sensing*.

Turner, Darren, Arko Lucieer, and Christopher Watson. 2012. “An Automated Technique for Generating Georectified Mosaics from Ultra-High Resolution Unmanned Aerial Vehicle

(UAV) Imagery, Based on Structure from Motion (SfM) Point Clouds." *Remote Sensing* 4 (12): 1392–1410. doi:10.3390/rs4051392.

Westoby, M.J., J. Brasington, N.F. Glasser, M.J. Hambrey, and J.M. Reynolds. 2012. "'Structure-from-Motion' Photogrammetry: A Low-Cost, Effective Tool for Geoscience Applications." *Geomorphology* 179 (December). Elsevier B.V.: 300–314. doi:10.1016/j.geomorph.2012.08.021.

Zhang, Yongjun, Jinxin Xiong, and Lijuan Hao. 2011. "Photogrammetric Processing of Low-Altitude Images Acquired by Unpiloted Aerial Vehicles." *Photogrammetric Record* 26 (134): 190–211. doi:10.1111/j.1477-9730.2011.00641.x.